



UNIVERSITÀ
DEGLI STUDI
FIRENZE

FLORE

Repository istituzionale dell'Università degli Studi di Firenze

Modelling and simulation of phase change material latent heat storages applied to a solar-powered Organic Rankine Cycle

Questa è la versione Preprint (Submitted version) della seguente pubblicazione:

Original Citation:

Modelling and simulation of phase change material latent heat storages applied to a solar-powered Organic Rankine Cycle / Manfreda, Giampaolo; Secchi, Riccardo; Stańczyk, Kamil. - In: APPLIED ENERGY. - ISSN 0306-2619. - STAMPA. - 179:(2016), pp. 378-388. [10.1016/j.apenergy.2016.06.135]

Availability:

The webpage <https://hdl.handle.net/2158/1044069> of the repository was last updated on 2021-04-09T12:02:04Z

Published version:

DOI: 10.1016/j.apenergy.2016.06.135

Terms of use:

Open Access

La pubblicazione è resa disponibile sotto le norme e i termini della licenza di deposito, secondo quanto stabilito dalla Policy per l'accesso aperto dell'Università degli Studi di Firenze (<https://www.sba.unifi.it/upload/policy-oa-2016-1.pdf>)

Publisher copyright claim:

Conformità alle politiche dell'editore / Compliance to publisher's policies

Questa versione della pubblicazione è conforme a quanto richiesto dalle politiche dell'editore in materia di copyright.

This version of the publication conforms to the publisher's copyright policies.

La data sopra indicata si riferisce all'ultimo aggiornamento della scheda del Repository FloRe - The above-mentioned date refers to the last update of the record in the Institutional Repository FloRe

(Article begins on next page)

Modelling and Simulation of Phase Change Material latent heat storages applied to a Solar-powered Organic Rankine Cycle

Giampaolo Manfrida ^{a,*}, Riccardo Secchi ^a, Kamil Stańczyk ^b

^a Department of Industrial Engineering - DIFE - University of Florence, Viale G. Morgagni, 40-44 – 50135 Florence, Italy

^b Silesian University of Technology, Institute of Thermal Technology, Konarskiego 22, 44-100 Gliwice, Poland

* E-mail corresponding Author: manfrida@unifi.it

Abstract

Solar energy is one of the most promising renewable energy sources, but is intermittent by its nature. The study of efficient thermal heat storage technologies is of fundamental importance for the development of solar power systems. This work focuses on a robust mathematical model of a Latent Heat Storage (LHS) system constituted by a storage tank containing Phase Change Material spheres. The model, developed in EES environment, provides the time-dependent temperature profiles for the PCM and the heat transfer fluid flowing in the storage tank, and the energy and exergy stored as well.

A case study on the application of the LHS technology is also presented. The operation of a solar power plant associated with a latent heat thermal storage and an ORC unit is simulated under dynamic (time-varying) solar radiation conditions with the software TRNSYS. The performance of the proposed plant is simulated over a one week period, and the results show that the system is able to provide power in 78.5% of the time, with weekly averaged efficiencies of 13.4% for the ORC unit, and of 3.9% for the whole plant (from solar radiation to net power delivered by the ORC expander).

Keywords: PCM; Latent Heat Storage; EES; TRNSYS; Solar energy; ORC

1. Introduction

Energy storage systems play a fundamental role in an effective development of renewable energy technologies, which are based on energy sources intermittent by their nature. The energy associated to the solar radiation is usually directly converted into two forms of energy: electricity (through photovoltaic panels) or thermal energy (using solar thermal collectors). Electricity storage technologies are usually classified according to their optimum application [1]: low-power application in isolated areas, medium-power application in isolated areas, network connection application with peak levelling, power-quality control applications. In the first two application the energy can be stored as kinetic energy (flywheel [2]), chemical energy (batteries [3, 4]), compressed air [5, 6], hydrogen (electrolyser), supercapacitors [7] or superconductors [8]; in large-scale systems energy is most effectively stored as gravitational energy (pumped hydro storage [9]), chemical energy (accumulators, flow batteries [10]) or compressed air.

Thermal energy storages for solar thermal applications can be divided into two main classes [11]: Sensible Heat Storages (SHS) and Latent Heat Storages (LHS). Phase Change Materials (PCMs) belong to the second class, and are among the most promising technologies to support the development of efficient Thermal Energy Storage (TES) systems. The efficiency of a TES is commonly defined as the ratio of the energy provided to the user and the energy needed to charge the storage system. It accounts for the energy losses during the storage period and the

charging/discharging cycle. In LHS systems thermal transfer occurs mainly when a storage material undergo a phase change: from solid to liquid, liquid to gas or solid to solid. PCMs can store 5-14 times more heat per unit volume than sensible-heat storage materials [12]. Moreover the process of phase change is almost isothermal for pure substances, and occurs over a finite range of temperature for composite materials, which is often an advantage compared to SHS systems. Solid-liquid transition proved to be the most economically attractive solution for LHS [12, 13, 15], due to the capability to store a relatively large amount of thermal energy within a narrow temperature range, without a large volume change [14]. However, the research and development conducted in the past showed also disadvantages concerning the low thermal conductivities typical of many PCMs, resulting in low rates of the charging and discharging processes [16].

In order to make the best of latent heat storage it is essential that a proper PCM is selected for the specific application, as the operating conditions are widely variable. A preliminary step in the design of any PCM system is the knowledge of material properties [17]. Many Phase Change Materials are available in different transition temperature ranges. A basic classification of solid-liquid PCMs considers the subdivision into organic, inorganic and eutectics [12, 18]. Organic PCM have some common qualities: they melt congruently, crystallize with little or no super cooling and are usually non-corrosive [19, 20]. They consist basically in Paraffinic and Non-Paraffinic compounds. Inorganic PCM generally have higher volumetric latent heat storage capacity than organic compounds. They consist of salt hydrates, fused/molten salts and metals. Eutectics are alloys of inorganic and/or organics having a single melting temperature, which is usually lower than that of any of the constitutive compounds. They are able to melt/freezing congruently without phase segregation [14].

The melting temperature is the main parameter to be considered for an appropriate selection of the PCM: it has to lie within the practical range of the selected application. Agyenim et al.[16] presented an overview of the PCM properties and related applications studied in literature. The applications were subdivided in three subclass in terms of operating temperature range:

- Low temperature: 0-65°C . Suitable PCMs are Paraffins, water/ice, stearic acid, n-octadecane;
- Medium temperature: 80-120°C. Appropriate PCMs are Erythritol, RT100, $\text{MgCl}_2 \cdot 6\text{H}_2\text{O}$;
- High temperature: > 150°C. Adequate PCMs are NaNO_3 , KNO_3 , NaOH , KOH , ZnCl_2 .

Several researchers studied the fluid flow and heat exchange inside a packed bed storage unit filled with encapsulated PCM. The first group of governing equations for the heat transfer between a packed bed of rocks and an HTF was proposed by Schumann [21] in 1929. In the last 20 years other authors proposed adapted model for a LHS system. Ismail et al. [22] presented a simplified transient one-dimensional model based on dividing a storage vessel into a number of axial layers with thickness equal or larger than the PCM capsule diameter. They assumed a uniform HTF's temperature equal to the average temperature of the layer, neglecting the heat loss through the vessel wall and the variation of the HTF temperature along the radial direction.

Wei et al. [23] modelled the heat exchange in the storage vessel assuming one dimensional heat transfer along the flow direction, considering the vessel completely insulated and neglecting internal natural convection (buoyancy). They also studied the heat transfer process inside the PCM, developing a conductive one-dimensional phase change model for the simulation of the solidification process of the PCM inside four types of capsule: sphere, cylinder, plate and tube.

Regin et al. [24] used the fundamental equations of Schumann except for the modelling of the phase change phenomena of the PCM inside the capsule, which was analyzed using the enthalpy instead of the temperature as reference quantity. They considered axial flow of an incompressible fluid inside a completely insulated vertical tank, assuming fixed bed porosity and constant thermo-physical properties of the HTF. The model was developed in the hypothesis of temperature variation only along the axial direction (no temperature variation in radial direction).

Wu et al. [25] presented a model of the dynamic discharging process of a spherical capsule packed bed storage system using Paraffin as the PCM and water as the HTF. The governing equations

written for the heat transfer process inside the storage vessel were based on the following assumptions: negligible temperature variation in radial direction for both PCM and HTF, constant thermo physical properties, PCM treated as a continuous medium, fully developed flow profile in axial direction.

Flueckiger et al. [27] presented a simulation of a Molten-salt thermocline tank filled with a bed of encapsulated PCM. The proposed system is an energy storage solution for concentrating solar power plants. They followed a finite-volume approach to simulate mass and energy transport inside the vessel, integrating the storage model into a system-level model of a molten-salt power tower plant to test the tank operation with respect to realistic solar collection and power production.

Tumilowicz et al. [28] used an enthalpy-based version of the Schumann equations to model the interactions throughout the thermocline processes. The method of characteristics was applied for the numerical solution. Vertical flow with uniform radial distribution of the fluid was considered, and the thermo-physical properties were assumed invariant with temperature. A lumped capacitance assumption is applied to the encapsulated PCM due to the low Biot number characterizing small size capsules.

Bedecarrats et al. investigated the performance of encapsulated PCM energy storage both from the experimental [40] and numerical [41] point of view. They considered spherical capsules containing water with a nucleation agent as PCM, and an aqueous solution of monoethylene glycol as heat transfer fluid. The model was developed considering the delay of the crystallization of the PCM (super cooling phenomenon), showing substantial agreement with the presented experimental results.

Among all possible applications of phase change materials, the present study covers one of the most promising, the association of the thermal storage device with a solar thermal plant powering an Organic Rankine Cycle (ORC) unit. The storage system is designed to operate at medium temperature (100-120°C). In particular, the flow of the heat transfer fluid (HTF) inside a cylindrical vessel filled with encapsulated spheres of PCM was analytically modelled and the storage charging and discharging phases have been analyzed from the energy and exergy point of views. The PCM material considered is a pure substance (phase transition is modelled as isothermal); this corresponds to the fundamental requirement of correct matching with a saturated vapour ORC cycle (the current technological system solution for a small-power application), where most of the heat must be provided to the ORC at constant temperature.

This allows building a complete transient model of the thermal storage system. The model is first of all validated through a comparison with literature experimental data, then some storage charge and discharge phases typical of a solar power plant are simulated with TRNSYS, and the results discussed. The TRNSYS simulation concerns the application of the TES to a solar powered Organic ORC unit. Several authors have proposed and analyzed solar ORC systems, but few of them have studied the coupling with energy storage systems. Calise et al. [44] presented the simulations and performance analysis of a regenerative and superheated ORC powered by a solar power plant made by concentrated parabolic trough (CPC) collectors. The developed simulation model was used as preliminary design tool in order to define the working fluid and the heat exchangers design. A global plant optimization was also performed considering the total cost of the plant as objective function.

Markides [45] proposed an overview of the technologies capable of converting the solar energy collected from low-concentration solar systems into useful power aimed at both domestic and industrial sectors (1-1000 kW). The author states that ORC systems are particularly well-suited to the conversion of low-to-medium-grade heat to electrical work at an output power scale from kilowatts to a few megawatts. Freeman et al. [46] simulated the performance of a small-scale combined solar heat and power (CSHP) system based on an ORC in order to assess the potential of the application of this technology for typical UK domestic users. The power output obtained from different type of solar collectors (concentrating parabolic-trough, evacuated tube) of the same total array area was compared, and a life-cycle cost analysis was also performed.

Bocci et al. [47] carried out a TRNSYS simulation of a solar residential tri-generative power plant composed of CPC solar thermal collectors (50 m^2), a thermal storage (3 m^3), an ORC (3 kWe), an adsorber (8 kWth) and a desalination device (200 l/h). The proposed system is able to produce power, heating/cooling and fresh water needs for a residential house.

Gang et al. proposed two configurations [48, 49] of low temperature solar thermal electric generation with regenerative ORC. The system proposed consists of non-tracking solar collectors and an ORC subsystem comprising evaporators, pumps, an organic fluid/heat storage tank with PCM, turbine, generator, regenerator, condenser and feed fluid heater. In contrast with a traditional solar ORC, the system uses an organic fluid/heat storage tank with a PCM set and two-stage evaporators. The first study [48] focuses on the impact of the regenerative cycle on the ORC efficiency and collector efficiency. In the second work [49] the authors studied in deep the configuration of the two-stage solar collectors (flat plate collectors, FPC, for the first stage and CPC for the second stage) and the corresponding PCM storages, establishing coupling relationship among the proportion of FPC to CPC, the melting temperature of the first-stage PCM and the overall collector efficiency.

The present work is divided in two parts:

(I) Development and description (Section 2) of a reliable analytical transient model of a Latent Heat Storage system. The storage configuration concerns a cylindrical tank filled with encapsulated spheres of PCM. A fluid flows through the PCM pack porosity, leading to melting (in charge phase) or solidification (in discharge phase) of the PCM. The model, developed in EES environment, allows to perform an energetic and exergetic analysis, and is validated against literature experimental results (Section 4).

(II) Simulation of the operation of a solar power plant associated with latent heat thermal storage and ORC unit under dynamic (time-varying) solar radiation conditions (Section 5). We consider, as a case study, a solar field composed of parabolic through collectors which feeds both the evaporator of a basic ORC and two LHS tanks installed in parallel. The dynamic simulation (over a 1 week period) of the system has been carried out coupling TRNSYS and EES. The EES model simulates the performance of the storages. The TRNSYS simulation time step (0.5 hours) corresponds to the EES total simulation time. The simulation results are also presented and discussed in Section 5.

2. Mathematical model

The typical configuration of a storage unit is shown in Figure 1. A cylindrical storage vessel is filled with spherical capsules containing a PCM. The charging and discharging processes are simulated considering an heat transfer fluid flowing through the porosity of the packed bed from the bottom to the top and vice versa. During the charging process the PCM undergoes a temperature rise in solid phase until the melting temperature of the PCM is reached; after this point, the melting process occurs at constant temperature. After complete phase change, the temperature of the liquid PCM can again increase up to the limit imposed by the HTF inlet temperature. Both sensible and latent heat fluxes are modelled. In the discharging phase the thermal energy stored in the PCM is removed by the “cold” HTF flowing through the packed bed in direction opposite to the charging phase; if superheated liquid conditions were reached, the PCM temperature first decreases up to the solidification temperature, which is maintained until complete phase change; the solid phase undergoes then a possible temperature reduction up to the limiting HTF inlet temperature.

Figure1

The governing equations for the heat transfer between PCM and HTF are based on the model proposed by Wu [25]. Some modifications were made, including heat losses to the environment (non-ideal insulation) and the presence of radial heat transfer with the storage vessel walls. The mathematical model is based on the following assumptions:

- The storage vessel is divided in N_x control volumes from the bottom to the top, each one having length dx .
- the thermo-physical properties of the PCM are constant for each physical state, while the properties of the HTF are temperature-dependent;
- the HTF fluid flow is fully developed in axial direction;
- the thermal resistance between the surface of the spherical capsules and PCM is neglected;
- the capsules have a single contact point, therefore the heat conduction between capsules is negligible;
- the effect of radial conduction is neglected, apart from the vessel boundary condition corresponding to non-adiabatic wall surface;
- the conduction of heat in the HTF in axial direction is negligible, due to the large Peclet number ($>>100$) achieved by the fluid flow in the storage tank [26].

The model consists of three main energy balance equations:

1. Phase Change Material:

$$(1-\varepsilon) \cdot \rho_P \cdot L \cdot \frac{\partial \phi}{\partial t} - (1-\varepsilon) \cdot \rho_P \cdot c_P \cdot \frac{\partial T_P}{\partial t} = h \cdot a_P \cdot (T_F - T_P) \quad (1)$$

where ε is the packed bed void fraction, ρ_P is density of the PCM, L is the heat of fusion per unit mass, ϕ is the PCM liquid fraction, c_P is the specific heat, h is the convective heat transfer coefficient between HTF and PCM, a_P is ratio between the total surface area of the spherical capsules and the tank internal volume, T_F is the HTF local temperature and T_P is the PCM local temperature.

Equation 1 represents the energy balance between the sensible and latent energy change of the PCM and the heat transfer from/to the HTF during the charging/discharging process.

In order to determine the PCM average state (solid, liquid, phase change), the liquid fraction ϕ is introduced: it represents the ratio between the liquid mass and the total mass of PCM.

Depending on the local instantaneous PCM temperature, this equation takes one of the following possible forms:

$$(T_P < T_{melt}) \wedge (\phi = 0) \Rightarrow (1-\varepsilon) \cdot \rho_{Ps} \cdot c_{Ps} \cdot \frac{\partial T_P}{\partial t} = h \cdot a_P \cdot (T_P - T_F) \quad (2)$$

$$(T_P = T_{melt}) \wedge (0 < \phi < 1) \Rightarrow (1-\varepsilon) \cdot \rho_{Ps} \cdot \lambda \cdot \frac{\partial \phi}{\partial t} = h \cdot a_P \cdot (T_P - T_F) \quad (3)$$

$$(T_P > T_{melt}) \wedge (\phi = 1) \Rightarrow (1-\varepsilon) \cdot \rho_{Pl} \cdot c_{Pl} \cdot \frac{\partial T_P}{\partial t} = h \cdot a_P \cdot (T_P - T_F) \quad (4)$$

2. Heat Transfer Fluid

$$\varepsilon \cdot \rho_F \cdot c_F \cdot u \cdot \frac{\partial T_F}{\partial x} = h \cdot a_P \cdot (T_F - T_P) + h_{F-ST} \cdot a_{ST} \cdot (T_F - T_{STW}) \quad (5)$$

where a_{ST} is lateral surface of the storage vessel per unit volume [1/m], h_{F-ST} is the convective heat transfer coefficient between the fluid and the storage vessel surface and T_{ST} is the local vessel wall temperature. The term on the left hand side of the Equation 5 represents the energy change due to the HTF flow. The two terms on the right hand represent the energy transfer by convection between the HTF and the PCM, and the heat leak through the wall of the cylindrical container.

3. Storage Tank walls:

$$Z \cdot \rho_{ST} \cdot c_{ST} \cdot \frac{\partial T_{ST}}{\partial t} = h_{F-ST} \cdot a_{ST} \cdot (T_F - T_{ST}) - h_e \cdot a_{ST-e} \cdot (T_{ST} - T_\infty) \quad (6)$$

$$Z = \frac{V_{STe} - V_{STi}}{V_{STi}} = \left(\frac{d_{STe}}{d_{STi}} \right)^2 - 1 \quad (7)$$

$$A = \pi \cdot (R_{STe}^2 - R_{STi}^2) \quad (8)$$

where Z is the storage tank wall volume per tank internal volume, h_E is the convective heat transfer coefficient between the storage tank surface and surrounding ambient, A is the storage tank cross section area. The term on the left hand side of Equation 6 represents the transient energy change of the storage tank walls. The terms on the right hand represent the energy transfer by convection between the HTF and the container walls, and the amount of heat released to surroundings.

The packed bed average void fraction is calculated using the correlation proposed by Beavers et al. [18] for a randomly-packed bed:

$$\varepsilon = 0.4272 - 4.516 \cdot 10^{-3} \cdot \left(\frac{d_{STi}}{d_p} \right) + 7.881 \cdot 10^{-5} \cdot \left(\frac{d_{STi}}{d_p} \right)^2 \quad (9)$$

Equation 9 shows the dependence of the void fraction from the ratio between the storage tank internal diameter d_{STi} , and the PCM capsule diameter d_p .

The heat transfer coefficient characterizing the convective heat transfer between the PCM and the HTF (h) are obtained as follows:

$$h = j_H \cdot G \cdot C_F \cdot Pr^{-2/3} \quad (10)$$

$$j_H = 0.23 \cdot Re^{-0.3} \quad (11)$$

where j_H is the Colburn factor [30], G is the specific HTF mass flow rate, Re is the Reynolds number calculated referring to the hydraulic radius for a matrix of spheres as suggested by Ackermann [31], Pr is the HTF Prandtl number.

The convective heat transfer between the HTF and the Storage tank wall was obtained using the internal pipe flow procedure proposed by Nellis and Klein [32]. The procedure presented by Nellis and Klein for free convection over a vertical cylinder was applied in the calculation of the external heat transfer coefficient between the external wall of the storage tank and the ambient air.

The model also includes exergy analysis and efficiency factors calculations. The following equations was written considering the local temperatures of PCM (T_P), HTF (T_F) and storage wall (T_{ST}). Moreover the rates of energy and exergy were considered. Therefore the quantities related to the whole storage tank and total charging/discharging cycle can be calculated integrating in x and t the local values.

The exergy flow balance for the storage system can be written as [36, 37]:

$$\dot{E}_{stored} = \dot{E}_{in} - \dot{E}_{out} - \dot{E}_Q - \dot{E}_d \quad (12)$$

where \dot{E}_{in} is the rate of exergy input, \dot{E}_{out} is the rate of exergy output, \dot{E}_Q is the rate of exergy loss due to heat transfer to the storage wall and environment, \dot{E}_d is the rate of exergy destruction. The difference between \dot{E}_{in} and \dot{E}_{out} can be referred as the storage exergy input rate.

The rate of exergy stored by the PCM \dot{E}_{stored} can be calculated integrating in x the local value [37, 38]:

$$d\dot{E}_{stored} = d\dot{Q}_{stored} \cdot \left(1 - \frac{T_o}{T_P} \right) \quad (13)$$

where the rate of energy stored ($d\dot{Q}_{stored}$) for each calculation time step Δt can assume the following forms depending on the local PCM temperature:

$$d\dot{Q}_{stored} = \begin{cases} (T_P < T_{melt}) \wedge (\phi = 0) \Rightarrow m_P \cdot c_{Ps} \cdot (T_{Ps\ fin} - T_{Ps\ ini}) \cdot (1/\Delta t) \\ (T_P = T_{melt}) \wedge (0 < \phi < 1) \Rightarrow m_P \cdot \lambda \cdot (\phi_{fin} - \phi_{ini}) \cdot (1/\Delta t) \\ (T_P > T_{melt}) \wedge (\phi = 1) \Rightarrow m_P \cdot c_{Pl} \cdot (T_{Pl\ fin} - T_{Pl\ ini}) \cdot (1/\Delta t) \end{cases} \quad (14)$$

The terms on the right hand side of Equation 12 can be computed from the following relations (here shown at differential level):

$$d\dot{E}_{in} - d\dot{E}_{out} = \dot{m}_F \cdot c_F \cdot \left[(T_{F\ in} - T_{F\ out}) - T_o \cdot \ln \left(\frac{T_{F\ out}}{T_{F\ in}} \right) \right] \quad (15)$$

$$d\dot{E}_Q = d\dot{Q}_{loss} \cdot \left(1 - \frac{T_o}{T_F} \right) \quad (16)$$

$$d\dot{E}_d = T_o \cdot s_{gen} \quad (17)$$

where the local heat loss rate ($d\dot{Q}_{loss}$) for each dx , and the local Entropy generation rate, \dot{s}_{gen} , are calculated as [39]:

$$d\dot{Q}_{loss} = h_{F-ST} \cdot (T_F - T_{ST}) \cdot \pi \cdot d_{STi} \quad (18)$$

$$d\dot{s}_{gen} = (d\dot{s}_{out} - d\dot{s}_{in}) + d\dot{s}_P + d\dot{s}_{ST} + \frac{d\dot{Q}_{loss}}{T_o} \quad (19)$$

$$(d\dot{s}_{out} - d\dot{s}_{in}) = \dot{m}_F \cdot c_F \cdot \ln \left(\frac{T_{Fout}}{T_{Fin}} \right) \quad (20)$$

$$d\dot{s}_P = \begin{cases} (T_P < T_{melt}) \wedge (\phi = 0) \Rightarrow m_P \cdot c_{Ps} \cdot \ln(T_{P\ fin}/T_{P\ ini}) \cdot (1/\Delta t) \\ (T_P = T_{melt}) \wedge (0 < \phi < 1) \Rightarrow m_P \cdot \lambda \cdot [(\phi_{fin} - \phi_{ini})/T_{melt}] \cdot (1/\Delta t) \\ (T_P > T_{melt}) \wedge (\phi = 1) \Rightarrow m_P \cdot c_{Pl} \cdot \ln(T_{P\ fin}/T_{P\ ini}) \cdot (1/\Delta t) \end{cases} \quad (21)$$

$$d\dot{s}_{ST} = m_{ST} \cdot c_{ST} \cdot \ln(T_{ST\ fin}/T_{ST\ ini}) \cdot (1/\Delta t) \quad (22)$$

In order to evaluate the performance of the storage device, three indicators are introduced. The Storage Energy Efficiency η_{ST-en} is given by:

$$\eta_{ST-en} = \frac{\int_0^X \int_0^\tau d\dot{Q}_{stored} \, dxdt}{\int_0^X \int_0^\tau d\dot{Q}_{stored} + d\dot{Q}_{loss} \, dxdt} \quad (23)$$

The Storage Exergy Efficiency η_{ST-ex} is:

$$\eta_{ST-ex} = \frac{\int_0^X \int_0^\tau d\dot{E}_{stored} \, dxdt}{\int_0^X \int_0^\tau d\dot{E}_{in} - d\dot{E}_{out} \, dxdt} \quad (24)$$

and finally a Storage Latent Efficiency η_{ST-lat} , used to quantify the fraction of energy stored as latent heat, can be defined as:

$$\eta_{ST-latent} = \frac{\int_0^X \int_0^\tau d\dot{Q}_{stored-pc} dx dt}{\int_0^X \int_0^\tau d\dot{Q}_{stored} dx dt} \quad (25)$$

where $\dot{Q}_{stored-pc}$ is the rate of energy stored during the phase transition.

3. Numerical solution

The model was developed in EES (Engineering Equation Solver) environment [33]. The convective heat transfer coefficients [32] were obtained using dedicated software internal libraries.

The model calculations are performed using a finite difference discretization in time and space (x longitudinal direction). Therefore the overall length of the storage tank is divided into N_x parts, and the simulation time τ into N_t intervals:

$$N_x = \frac{X}{\Delta x} ; \quad N_t = \frac{\tau}{\Delta \tau} \quad (26)$$

In Equations 24 X is the total tank length, τ is the total simulation time.

It is worth to point out that respecting the Courant–Friedrichs–Lewy (CFL) condition [34] is recommended for the stability and accuracy of the results in a time-dependent calculation. For the one-dimensional case, the CFL has the following form:

$$u \cdot \frac{\Delta \tau}{\Delta x} \leq 1 \quad (27)$$

where u is the HTF flow velocity.

The discretized mathematical equations become:

$$1. \text{ PCM} \quad (1-\varepsilon) \cdot \rho_P \cdot L \cdot \frac{\phi_i^j - \phi_i^{j-1}}{\Delta \tau} - (1-\varepsilon) \cdot \rho_P \cdot C_P \cdot \frac{T_{Pi}^j - T_{Pi}^{j-1}}{\Delta \tau} = h \cdot a_P \cdot (T_{Fi}^j - T_{Pi}^j) \quad (28)$$

$$2. \text{ HTF} \quad \varepsilon \cdot \rho_F \cdot C_F \cdot u \cdot \frac{T_{Fi}^j - T_{Fi-1}^{j-1}}{\Delta x} = h \cdot a_P \cdot (T_{Fi}^j - T_{Pi}^j) + h_{F-ST} \cdot a_{ST} \cdot (T_{Fi}^j - T_{STi}^j) \quad (29)$$

$$3. \text{ ST} \quad Z \cdot \rho_{ST} \cdot C_{ST} \cdot \frac{T_{STi}^j - T_{STi-1}^{j-1}}{\Delta \tau} = h_{F-ST} \cdot a_{ST} \cdot (T_{Fi}^j - T_{STi}^j) - h_e \cdot a_{ST-e} \cdot (T_{STi}^j - T_\infty) \quad (30)$$

where: $i=0, \dots, N_x$ and $j=0, \dots, N_t$.

Table 1

Figure 2

Table 1 shows the initial and boundary conditions applied in the charging and discharging simulations. At the inlet of packed bed, the HTF is assumed to be at constant temperature (T_{inlet}). At the beginning of the first charging process, the temperatures of the PCM and HTF are equal to the ambient temperature. The initial values for the discharging process are imported from the final results of the charging simulation (last time step, N_t), assuming adiabatic behaviour of the vessel. The numerical solution of the governing equations follows the order depicted in Figure 2.

4. LHS Model Validation

The thermodynamic model of the LHS is validated comparing the numerical results with the experimental data presented by Nallusamy et al. [35], who investigated the thermal behaviour of a packed bed LHS integrated in a solar collector circuit. The properties of the considered PCM spheres, HTF and storage tank are shown in Table 2. The storage tank is assumed to be made of stainless steel.

A comparison between experimental and simulated HTF temperature variation at the tank outlet section ($x/X=1$) is presented in Figure 3. The absolute discrepancy between the compared values is also shown in Figure 3 as a histogram (right scale). The temperature profiles are in good agreement: the absolute difference does not exceed 10 K over the whole charging process. As can be seen, the main differences stem from:

- (I) the hypothesis of constant temperature phase transition: when the melting temperature (333 K) is reached, the numerical temperature profile shows a constant value for the duration of the phase transition. The experimental profile does not show constant temperature sections.
- (II) the timing of the HTF temperature growth: the highest temperature difference occurs in the initial period (time < 0.5 hours) when the fluid temperature profiles show a higher slope.

In the first part of the numerical profile (0.15 hours) the HTF temperature at the storage outlet is constant due to the initial condition on the fluid temperature inside each spatial section of the storage. The numerical profile shows some small sudden local variations due to the discrete nature of the calculation and to the alternative management of computational models developed for the operations in the regions of sensible or latent heat.

The numerical model allows to reasonably predict the LHS performance; therefore it can be used to model the LHS as a component in a more complex plant.

Table 2

Figure 3

5. Case study – TRNSYS simulation

The software TRNSYS was used to simulate the operation of a solar power plant associated with latent heat thermal storage and ORC unit under time-varying solar radiation conditions. The quasi-steady TRNSYS model calls EES modules solving the LHS components with true dynamic behaviour, as was described in the previous sections.

A schematic diagram of the system is showed in Figure 4. The goal was to design a system capable of providing constant HTF power entering the evaporator of the ORC unit.

The proposed plant comprises the following components:

1. A solar collector field: NEP SOLAR parabolic trough collectors [42, 43] were considered.
2. Two latent heat storage tank (A, B) in parallel. This configuration allows to manage the storages discharge with the aim to provide a constant power to the ORC evaporator. Erythritol ($C_4H_{10}O_4$) was chosen as PCM, and pressurized water as HTF (15 bar). Charging and discharging phases are simulated through successive calls to the EES models of the storage tanks. EES imports necessary input data from TRNSYS (HTF temperature and flow rate) as well as latest data profile (T , Φ , Q_{stored} , E_{stored}) of the vessel, performs calculations and exports the results back to TRNSYS for each simulation time step.
3. Basic ORC plant (evaporator, expander, condenser, and pump): in the TRNSYS model the main control parameter is the thermal power provided to the ORC evaporator.

4. Control system: the control logic of the system described in the next paragraph is implemented through a system of solenoid valves.

Figure 4

The main properties of the plant components are listed in Table 3.

5.1 System operation

Each module of the TRNSYS model is switched on or off by logical functions depending on several simulation parameters, thus implementing the desired system control logic.

The operation phases of the storage system are defined as charging phase (CP) and discharging (DP) phase. The initial temperature profile in the vessels is generated at the beginning of the simulation. The value of ambient temperature is imported directly from the TRNSYS weather data module.

Table 3

In the first day of simulation, the system focuses only on charging both storage tanks and there is no power generation yet (V1,V2 are closed; this corresponds to a “cold start” of the system). The “cold start” is a difficult initial condition for the model, which serves also to verify its robustness. During the “standard” day, HTF is being directed to both latent heat storage systems (A, B) as well as straight to ORC evaporator. At night the power is provided from discharging the vessels (one at a time) with constant HTF flow. The same order applies to remaining days simulated. Table 4 summarizes the operation phases for the standard simulation day.

Table 4

The HTF flow rate through the storage tanks in a standard day charging phase follows the Load Profile shown in Figure 5 (Total Collectors flow rate, \dot{m}_{TOT}) minus a Bypass flow rate ($\dot{m}_{BP-ORC} = 3$ kg/s) flowing continuously through valve V2. In the EES modules modelling the LHS it was not possible to change dynamically the number of time-steps (N_t) with variable HTF flow rate (determined by the main TRNSYS simulation). N_t was therefore set to satisfy the CFL condition considering the highest value of flow rate for each storage tank (Profile $[CP]Tank A=B$ in Figure 5). The Total Collectors flow rate profile was set with the aim to maintain a minimum flow through the solar field even when there is no storage tank charging or flow through the by-pass. In this case, V1 is open, while V2,V3 and V4 are closed: the flow rate in the solar collector field corresponds to the *By-Pass SC* profile in Figure 5.

In the discharge phase the HTF temperature at evaporator outlet is assumed to be constant and equal to $T_{EV,out} = 370K$, while the inlet temperature is time-varying and equal to the temperature of the fluid at storages outlet during the discharging phase. The HTF flow rate in the discharge phase was set to $\dot{m}_{DP} = 4$ kg/s. The duration of the discharging phase of storage tank B is not defined a priori. It depends on the conditions described in the third column of Table 4. Tank B discharge stops when the fluid outlet temperature is lower than the PCM melting temperature. This concept is outlined in Table 4 through the symbol *B/D/stop* replacing the final hour of the day of Tank B discharging phase and, consequently, the initial hour of the day of Tank A discharging.

Figure 5

5.2 Results of dynamic simulations

In this section, we present the results of the dynamic TRNSYS simulations. Pisa San Giusto (Italy, N43°40', E10°23') was selected as the reference location, while the simulation time step was set to 0.5 hour. The TRNSYS simulation time step corresponds to the total simulation time (τ) of the EES module modelling the storage tank charge and discharge processes. One full week was simulated in order to evaluate the performance of the plant under different weather conditions (third week of July).

Figure 6 shows the temperature variation at the storage tanks inlet and outlet sections during the charging and discharging phases of the simulated period. The operational phases (CP, DP) are highlighted through different background colour. Due to the “cold start” initial conditions discussed in the previous paragraph, in the first day the discharge phase is not activated. The outlet temperature of both storages is similar in each time step of the charging phase, thus the corresponding profiles in Figure 6 are almost completely overlapped. In each charging phase the tanks outlet temperatures show a constant profile after an initial growth: this is due to the phase transition of the PCM.

The storage tanks inlet temperature in the discharge phase is always equal to 370 K, which is the imposed ORC evaporator outlet temperature.

The Latent heat storage system is designed to work at the temperature of PCM phase transition. As it can be seen, that largest part of the charging and discharging process actually occurs at 390 K. In particular, in the charging phase the storage system (both tanks) works at the temperature of PCM phase transition (i.e. latent heat storage) for about 70% of the operation time, while in the discharge phase this percentage falls to 40% due to the discharging limit of Tank A (370K), which allows the system to discharge the storages in the sensible heat region.

However, considering the operation period in which the storage system works at a temperature in the range $[T_{\text{melting}} - 3\text{K} ; T_{\text{melting}} + 3\text{K}]$, the percentages grow to about 81% and 87% respectively. This confirms that the storage system is able to supply the HTF at a nearly constant temperature for most of the operational time.

Figure 6

The profiles of energy and exergy stored in the tanks are shown in Figure 7 a, b. The storage system operational phases are clearly highlighted by the increase or reduction of the energy stored.

The amount of energy stored during the week varies between 6 and 20 GJ, depending on the daily radiation, while the exergy stored ranges between 1.2 and 4 GJ.

The weekly-averaged values of the storages Energy and Exergy efficiencies of the PCM storages, defined according to Eqs. 23 and 24, are reported for the different operational phases in Table 5. The average Energy efficiency varies from about 83% in the charging phase to about 93% in the discharge phase, while the average Exergy efficiency is about 68% for both different storage tanks and different operational phases. The differences between the two storages arise from the different operation periods in discharging phase, which affect the subsequent charging phase as well.

Figure 7

The smaller average efficiencies obtained in charging phase are affected by the operation of the fourth simulation day: the energy stored in both tanks is reduced if compared to the other days due to the low temperature available at collector outlet. Almost half of the PCM doesn't undergo phase change during the charging phase. On the other hand, the energy losses to the environment are not reduced by the same amount. For example, the daily averaged Energy efficiencies in CP for the storage tank A is about 59% for the fourth simulation day, while the other days show values close to 88%.

Table 5

A main indicator of the correct plant operation is the profile of thermal power available at the ORC evaporator (\dot{Q}_{REN}). According to the system control logic, the thermal power comes from the by-pass in the hours of the day between the 10 am and the 5.30 pm, but only if the exit temperature of the collector field is above 370K. After 5.30 pm the storages are discharged following the schedule described in Table 4, providing thermal power to the ORC evaporator. Figure 8 shows the different contribution to the thermal power available at the evaporator during the simulated week, and the total power.

Figure 8

The system provides an average thermal power of about 295 kW over the 6 days period (in the first day the system works only for the cold start charging of the storage). The system provides thermal power at the ORC evaporator in 113 of the 144 total hours (78.5%). In the fifth day of the simulation, the minimum daily working hours of the ORC were obtained (14 hours). This is due to the lack of solar radiation on the day before: the storage system is not adequately charged (the energy stored reaches a maximum of 11 GJ for each storage tank, as was shown in Figure 7), thus its contribution stops on the 96th simulation hour (midnight of the fourth day).

In order to evaluate the performance of the whole system without increasing the computational costs of the TRNSYS simulation, a simple ORC (calculated in an external EES file) was added to the model. The inputs of the additional simulation are the time profile of the HTF flow rate and temperature at inlet and outlet of the evaporator, thus the thermal power delivered to the ORC from the renewable energy source can be directly calculated. R245fa was considered as working fluid, and the evaporator pressure was set at 16 bars in order to ensure that saturated or slightly superheated vapour is present at the turbine inlet for all the thermal power inputs of the cycle. The pressure at the ORC condenser is about 1.5 bars, and the organic fluid flow rate varies in the range 1-1.5 kg/s according to the variation of the fluid temperature at the evaporator. The efficiencies of the ORC pump and turbine are assumed to be constant and equal to 0.8.

Three additional efficiency parameters have been defined:

$$\text{- An Average ORC Efficiency: } \eta_{ORC} = \frac{\int_0^{Tt} \dot{Q}_{ORC}}{\int_0^{Tt} \dot{Q}_{REN}} \quad (31)$$

where Tt is the TRNSYS total simulation time (168 hours), \dot{Q}_{ORC} is the net power generated by the ORC cycle, and \dot{Q}_{REN} is the thermal power supplied to the evaporator from the renewable energy source, either directly or indirectly through the storage system.

$$\text{- An Average Overall System Efficiency: } \eta_{SYS} = \frac{\int_0^{Tt} \dot{Q}_{ORC}}{\int_0^{Tt} \dot{Q}_{Solar}} \quad (32)$$

where \dot{Q}_{Solar} is the solar radiation collected by the solar plant (whose size is specified in Table 3).

$$\text{- An Average Collectors-to-Evaporator Efficiency: } \eta_{C-E} = \frac{\int_0^{Tt} \dot{Q}_{REN}}{\int_0^{Tt} \dot{Q}_{Solar}} \quad (33)$$

The weekly averaged values of the ORC Efficiency, Overall System Efficiency, and Collectors-to-Evaporator Efficiency resulted to be equal to 13.4% , 3.9%, and 29.6% respectively.

6. Conclusions

This work focused on creating a robust mathematical model of latent heat storage systems consisting in storage vessels containing packed PCM spheres. The model provides the time-dependent temperature profiles for the PCM and the heat transfer fluid flowing in each storage tank. The storage energy and exergy efficiencies were also defined in order to evaluate the performance of the storage system. The PCM storage model was validated against experimental results from literature data, showing a satisfactory agreement.

The model was then implemented within a solar powered ORC unit, in order to realize a storage system providing constant thermal power to the ORC cycle in periods of deficiency of solar radiation.

The dynamic performance of the overall system was simulated with a mixed TRNSYS/EES program, at time-varying weather conditions (solar radiation, ambient temperature), over a one-week period. The simulation proved that with the implementation of the heat storage system it is possible to design solar powered ORC plant generating an almost constant power: the thermal energy stored during the day can be used to provide energy at night and during periods of insufficient solar radiation. The storage system showed a weekly average Energy efficiency of about 83% in charging phase and 93% in discharging phase, while the average Exergy efficiency was about 68% for both the operational phases. The proposed plant allows generating power in 78.5% of the simulation period, with a weekly averaged overall efficiency of 3.9%. The thermal energy provided by the system (either directly from the solar collectors or indirectly through the storages) to the ORC evaporator is about 29.6% of the solar energy collected by the solar plant during the simulated week.

Significant improvements over this performance appear possible with more complex control logics for several components (solar collectors, storage, ORC load matching).

Future work should concentrate on defining appropriate control logics for the main system parameters, and performing the dynamic simulation of the system over a more extended period. The evaluation of the annual performance of the system would lead to a more robust performance prediction and, consequently, to an iterative re-design of the system components in order to define the optimal design for a given reference geographic position.

Acknowledgements

This work was developed through the collaboration between the Silesian University of Technology and the University of Florence, within the framework of an ERASMUS Programme.

Reference

- [1] Ibrahim H., Ilinca A., Perron J., "Energy storage systems-Characteristics and comparisons", *Renewable and Sustainable Energy Reviews* 2008;12:1221–1250.
- [2] Sebastián R., Pena Alzola R., "Flywheel energy storage systems: Review and simulation for an isolated wind power system", *Renewable and Sustainable Energy Reviews* 2012;16:6803–6813.
- [3] Yang Z, J Zhang, MCW Kintner-Meyer, X Lu, D Choi, JP Lemmon, and J Liu., "Electrochemical Energy Storage for Green Grid." *Chemical Reviews* 2011;111(5):3577-3613. doi:10.1021/cr100290v

- [4] Hu X., Xiong R., Egardt B., “Model-Based Dynamic Power Assessment of Lithium-Ion Batteries Considering Different Operating Conditions”, IEEE transactions on industrial informatics, 2014, Vol.10, No. 3.
- [5] Fiaschi D., Manfrida G., Secchi R., Tempesti D., “A versatile system for offshore energy conversion including diversified storage”, Energy 2012;48:566-576.
- [6] Manfrida G., Secchi R.,” Performance Prediction of a Small-Size Adiabatic Compressed-Air Energy Storage System”, International Journal of Thermodynamics (IJoT), 2015; Vol. 18 (No. 2):111-119, 2015.
- [7] Zhang L., Hu X., Wang Z., Sun F., Dorrell D. G., “Fractional-order modeling and State-of-Charge estimation for ultracapacitors”, Journal of Power Sources 2016;314:28-34.
- [8] Holla R.V., “Energy Storage Methods - Superconducting Magnetic Energy Storage - A Review”, Journal of Undergraduate Research 2015;5,1.
- [9] Manfrida G., Secchi R.,”Seawater pumping as an electricity storage solution for photovoltaic energy systems”, Energy 2014;69:470-484.
- [10] Alotto P., Guarnieri M., Moro F., “Redox flow batteries for the storage of renewable energy: A review”, Renewable and Sustainable Energy Reviews 2014;29:325–335.
- [11] Tian Y., Zhao C.Y. “A review of solar collectors and thermal energy storage in solar thermal applications”, Applied Energy 2013;104:538–553.
- [12] Sharma A., Tyagi V.V., Chen C.R., Buddhi D. “Review on thermal energy storage with phase change materials and applications”, Renewable and Sustainable Energy Reviews 2009;13:318–345.
- [13] Hasnain SM. “Review on sustainable thermal energy storage technologies, Part I: heat storage materials and techniques”, Energy Conversion and Management 1998;39:1127–38.
- [14] Tatsidjodoung P., Le Pierrès N., Luo L. “A review of potential materials for thermal energy storage in building applications”, Renewable and Sustainable Energy Reviews 2013;18:327–349.
- [15] Vélez C., Khayet M., Ortiz de Zárate J.M. “Temperature-dependent thermal properties of solid/liquid phase change even-numbered n-alkanes: n-Hexadecane, n-octadecane and n-eicosane”, Applied Energy 2015; 143:383–394.
- [16] Agyenim F., Hewitt N., Eames P., Smyth M. “A review of materials, heat transfer and phase change problem formulation for latent heat thermal energy storage systems (LHTESS)”, Renewable and Sustainable Energy Reviews 2010;14:615–628.
- [17] Jankowski N.R., McCluskey F. P. “A review of phase change materials for vehicle component thermal buffering”, Applied Energy 2014;113:1525–1561.
- [18] Zhou D., Zhao C. Y., Tian Y. “Review on thermal energy storage with phase change materials (PCMs) in building applications” Applied Energy 2012; 92:593-605.
- [19] Zalba B., Marin J.M., Cabeza L.F., Mehling H. “Review on thermal energy storage with phase change: materials, heat transfer analysis and applications”, Applied Thermal Engineering 2003; 23:251–283.
- [20] Cabeza L.F., Castell A., Barreneche C., de Gracia A., Fernández A.I. “Materials used as PCM in thermal energy storage in buildings: A review”, Renewable and Sustainable Energy Reviews 2011;15:1675–1695.
- [21] Schumann T.E. “Heat transfer: a liquid flowing through a porous prism” J.Franklin Institute 1929;208(3):405–16.
- [22] Ismail K.A.R., Henriquez J.R. “Numerical and experimental study of spherical capsules packed bed latent heat storage system”, Applied Thermal Engineering 2002;22:1705–1716.

- [23] Wei J., Kawaguchi Y., Hirano S., Takeuchi H. “Study on a PCM heat storage system for rapid heat supply”, *Applied Thermal Engineering* 2005; 25:2903–2920.
- [24] Regin A.F., Solanki S.C., Saini J.S. “An analysis of a packed bed latent heat thermal energy storage system using PCM capsules: Numerical investigation”, *Renewable Energy* 2009; 34:1765–1773.
- [25] Wu S., Fang G., Liu X. “Dynamic discharging characteristics simulation on solar heat storage system with spherical capsules using paraffin as heat storage material”, *Renewable Energy* 2011; 36:1190–1195.
- [26] Van Lew J., Li P.W., Chan C.L., Karaki W., Stephens J. “Transient heat delivery and storage process in a thermocline heat storage system”, *Proceedings of ASME 2009 International Mechanical Congress and Exposition*, November 13–19, 2009, Lake Buena Vista, FL, USA.
- [27] Flueckiger S.M., Garimella S.V. “Latent heat augmentation of thermocline energy storage for concentrating solar power – A system-level assessment”, *Applied Energy* 2014; 116:278–287.
- [28] Tumilowicz E., Chan C.L., Li P., Xu B. “An enthalpy formulation for thermocline with encapsulated PCM thermal storage and benchmark solution using the method of characteristics”, *International Journal of Heat and Mass Transfer* 2014; 79:362–377.
- [29] Beavers G.S., Sparrow E.M., Rodenz D. E. “Influence of Bed Size on the Flow Characteristics and Porosity of Randomly Packed Beds of Spheres”, *J. Applied Mechanics* 1973; 40(3):655–660.
- [30] Kays A., London A. “Compact heat exchangers”. 3rd ed. Ed. McGraw-Hill. New York, USA. 1984.
- [31] Ackermann R. “Cryogenic Regenerative Heat Exchangers”. Plenum Press, New York, 1997.
- [32] Nellis G.F., Klein S.A. “Heat Transfer”. Cambridge University Press, 2009.
- [33] EES, Engineering Equation Solver, website: <http://www.fchart.com/>.
- [34] Courant R., Friedrichs K., Lewy H. “On the partial difference equations of mathematical physics” *IBM Journal of Research and Development* 1967; 11(2):215–234.
- [35] Nallusamy N., Sampath S., Velraj R. “Experimental investigation on a combined sensible and latent heat storage system integrated with constant/varying (solar) heat sources”, *Renewable Energy* 2007; 32:1206–1227.
- [36] Ereǵ A., Dincer I., “An approach to entropy analysis of a latent heat storage module”, *International Journal of Thermal Sciences* 2008; 47:1077–1085.
- [37] Jegadheeswaran S., Pohekar S.D., Kousksou T., “Exergy based performance evaluation of latent heat thermal storage system: A review”, *Renewable and Sustainable Energy Reviews* 2010; 14:2580–2595.
- [38] Demirel Y., Öztürk H.H., “Thermoeconomics of seasonal latent heat storage system”, *Int. J. Energy Res.* 2006; 30:1001–1012.
- [39] MacPhee D., Dincer I., “Thermodynamic Analysis of Freezing and Melting Processes in a Bed of Spherical PCM Capsules”, *J. Sol. Energy Eng.* 2009; 131(3):031017–031017-11.
- [40] Bédécarrats J.P., Castaing-Lasvignottes J., Strub F., Dumas J.P., “Study of a phase change energy storage using spherical capsules. Part I: Experimental results”, *Energy Conversion and Management* 2009; 50:2527–2536.
- [41] Bédécarrats J.P., Castaing-Lasvignottes J., Strub F., Dumas J.P., “Study of a phase change energy storage using spherical capsules. Part II: Numerical modelling”, *Energy Conversion and Management* 2009; 50: 2537–2546.
- [42] Technical data of NEP SOLAR collectors, website: http://www.nep-solar.com/wp-content/uploads/2013/11/NEP-Solar-Polytrough1800_Datasheet.pdf (accessed 03/02/2016).

- [43] Test Report No. C1549LPEN. Performance test PolyTrough 1800. Rapperswil, Switzerland: SPF. Institut für Solartechnik; 2012. p. 16.
- [44] Calise F., Capuozzo C. Vanoli L., “Design and parametric optimization of an Organic Rankine Cycle powered by solar energy”, *American Journal of Engineering and Applied Sciences*, 2013; 6(2): 178-204.
- [45] Markides C.N., “Low-Concentration Solar-Power Systems Based on Organic Rankine Cycles for Distributed-Scale Applications: Overview and Further Developments.” *Front. Energy Res.* , 2015;3:47. doi: 10.3389/fenrg.2015.00047
- [46] Freeman J., Hellgardt K., Markides C.N., ”An assessment of solar-powered organic Rankine cycle systems for combined heating and power in UK domestic applications”, *Applied Energy* 2015; 138:605–620.
- [47] Bocci E., Villarini M., Vecchione L., Sbordone D., Di Carlo A., Dell’Era A., “Energy and economic analysis of a residential Solar Organic Rankine plant”, *Energy Procedia* 2015;81:558 – 568.
- [48] Gang P., Jing L., Jie J., “Analysis of low temperature solar thermal electric generation using regenerative Organic Rankine Cycle”, *Applied Thermal Engineering* 2010;30:998–1004.
- [49] Gang P., Jing L., Jie J., “Design and analysis of a novel low-temperature solar thermal electric system with two-stage collectors and heat storage units”, *Renewable Energy* 2011;36:2324-2333.

List of symbols

A	Storage vessel cross section area, m^2
a_P	Surface area of spherical capsules per volume, $1/m$
a_{ST}	Surface area of the vessel per unit volume, $1/m$ [$= 2/R_i$]
c	Specific heat, $J/(kg \cdot K)$
d	Diameter, m
e	Specific exergy, J/kg
\dot{E}	Flow exergy, W
G	Mass flow rate per unit section, $kg/(s \cdot m^2)$
h	Convective heat transfer coefficient between HTF and PCM, $W/(m^2 \cdot K)$
h_e	External Convective heat transfer coefficient between the storage vessel and the environment, $W/(m^2 \cdot K)$
h_{F-ST}	Convective heat transfer coefficient between the fluid and the storage vessel surface, $W/(m^2 \cdot K)$
j_H	Colburn factor [-]
k	Thermal conductivity, $W/(m \cdot K)$
\dot{m}	Flow rate, kg/s
N	Number of calculation steps
Pe	Peclet number
Pr	Prandtl number
\dot{Q}	Thermal Energy, W
R	Radius, m
Re	Reynolds number [-]
s	Entropy, $J/(kg \cdot K)$
t	Time, s
T	Temperature, K
u	Velocity, m/s
x	Axial coordinate, m
X	Total tank length, m
Z	Storage tank wall volume per tank internal volume [-]

Greek letters

Δx	Space interval, m
Δt	Time Interval, s
ε	Void fraction of packed bed [-]

λ	Heat of fusion per unit mass, J/kg
η	Efficiency
Φ	Liquid fraction of PCM [-]
ρ	Density, kg/m ³
τ	Total simulation time, s

Subscripts

<i>a</i>	Average
<i>e</i>	External
<i>en</i>	Energy
<i>ex</i>	Exergy
<i>F</i>	Heat transfer Fluid
<i>fin</i>	Final
<i>gen</i>	Generated
<i>i</i>	Internal
<i>in</i>	Inlet
<i>init</i>	Initial
<i>l</i>	Liquid
<i>lat</i>	Latent
<i>loss</i>	Loss
<i>melt</i>	Melting
<i>o</i>	Ambient
<i>out</i>	Outlet
<i>P</i>	Phase Change Material
<i>s</i>	Solid
<i>st</i>	Stored
<i>STW</i>	Storage Vessel Wall

Acronyms

<i>CFL</i>	Courant–Friedrichs–Lewy condition
<i>CP</i>	Charging Phase
<i>CPC</i>	Concentrated Parabolic Collector
<i>CSHP</i>	Combined Solar Heat and Power
<i>DP</i>	Discharging Phase
<i>EES</i>	Engineering Equation Solver
<i>HTF</i>	Heat Transfer Fluid
<i>LHS</i>	Latent Heat Storage
<i>ORC</i>	Organic Rankine Cycle
<i>PCM</i>	Phase Change Materials

<i>SHS</i>	Sensible Heat Storage
<i>TES</i>	Thermal Energy Storage
<i>TRNSYS</i>	Transient System Simulation Tool

Figure captions

Figure 1 - Schematic 1) longitudinal section, 2) heat transfer occurring and 3) cross section of the storage vessel

Figure 2 - Schematic visualization of the space-time solution approach

Figure 3 - Comparison between the present numerical simulation and experimental data in Ref. [35].

Figure 4 - Schematic diagram of the system with latent heat storage.

Figure 5 – HTF flow rate daily profiles in charging phase.

Figure 6 – Simulated Temperatures in different points of the storage system during the week.

Figure 7 – Energy (a) and Exergy (b) stored variation during the week.

Figure 8 – Thermal Power to ORC evaporator during the summer week simulated.

Figure 1

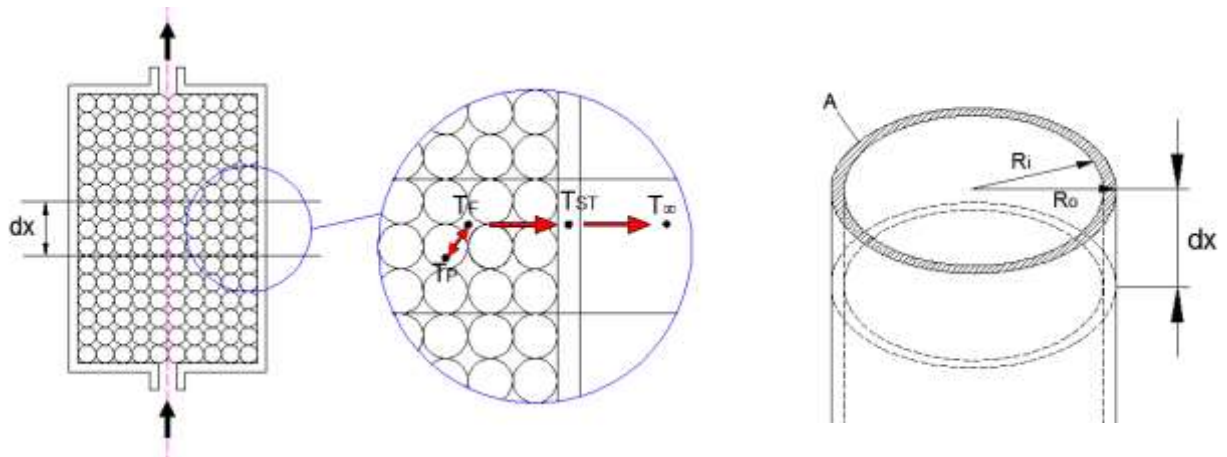


Figure 2

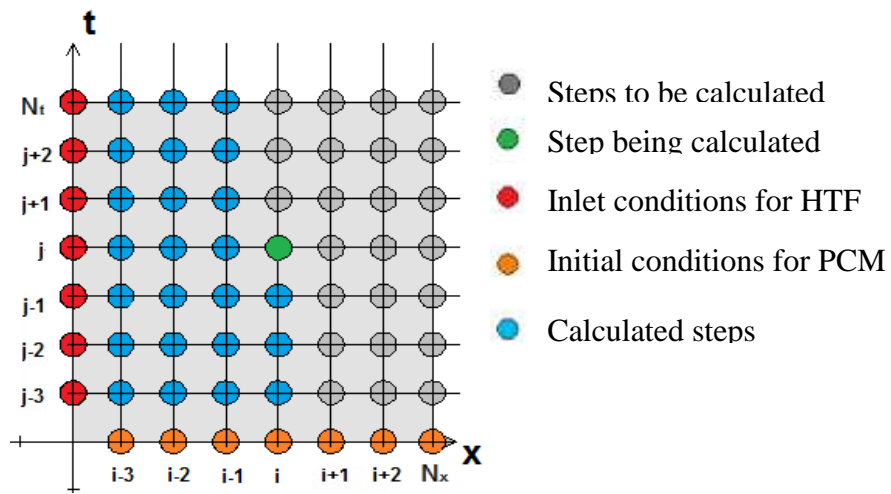


Figure 3

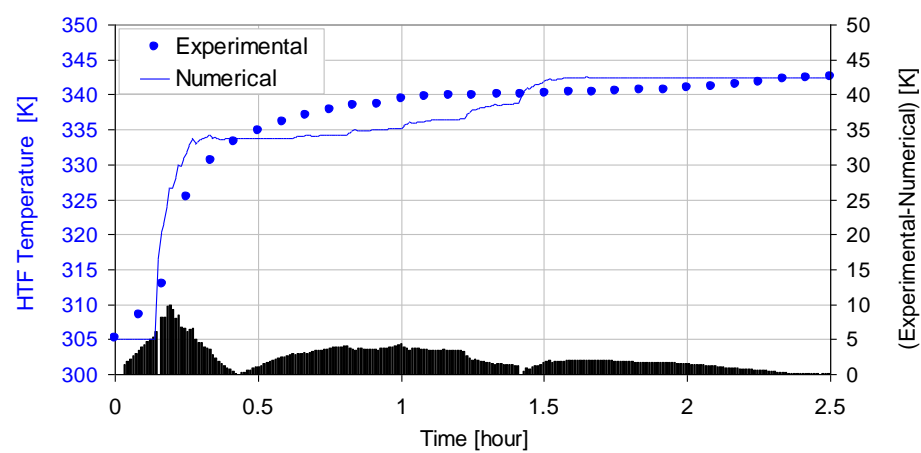


Figure 4

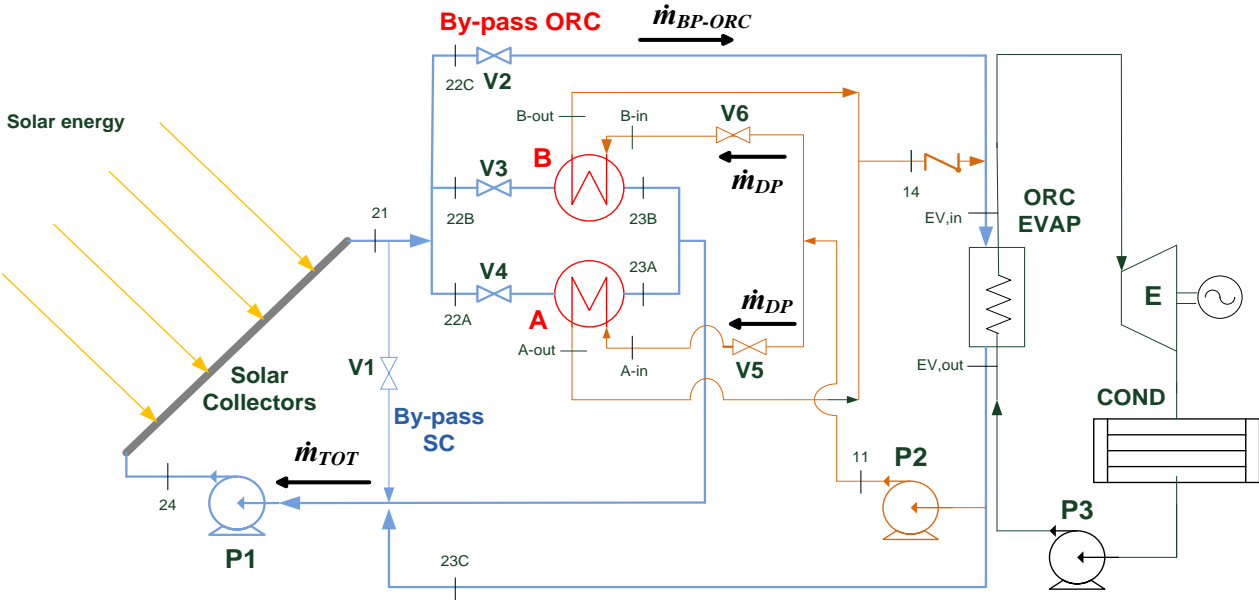


Figure 5

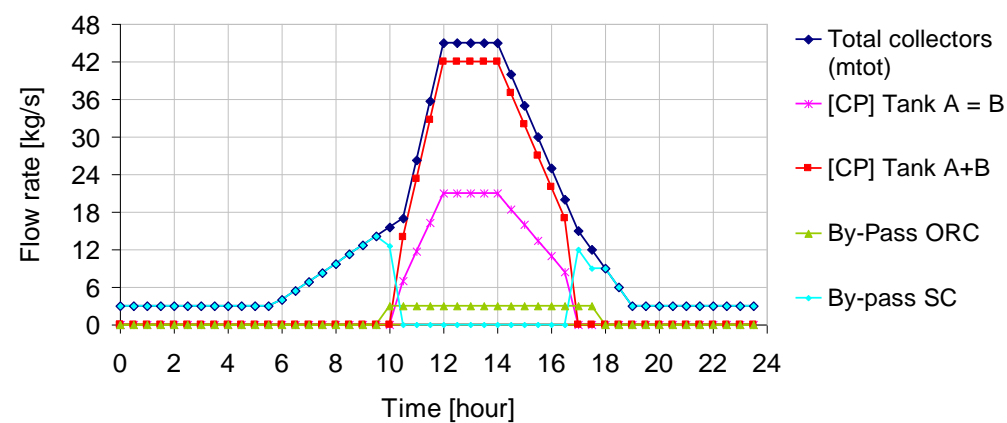


Figure 6

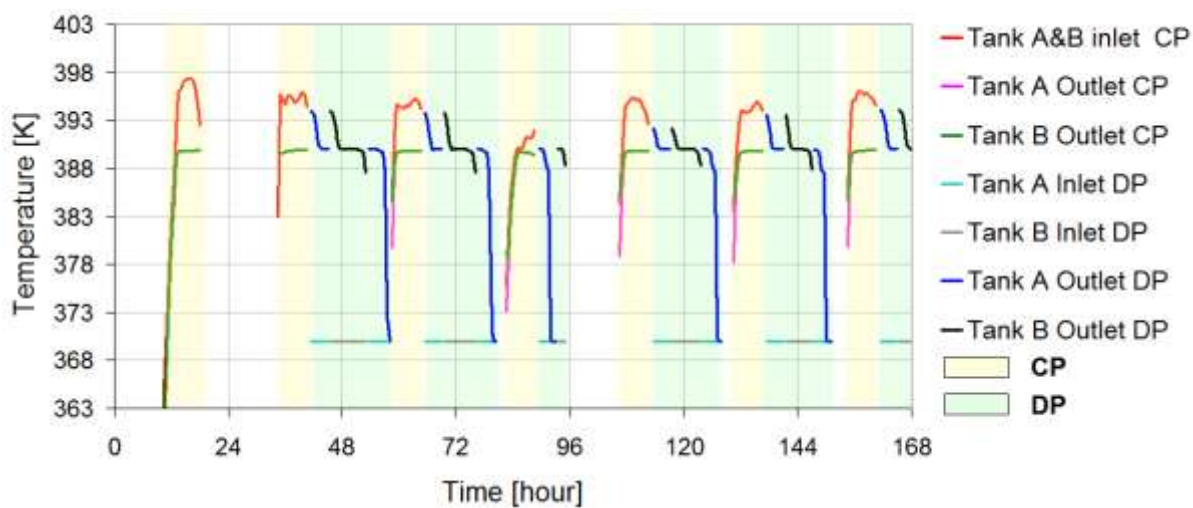


Figure 7

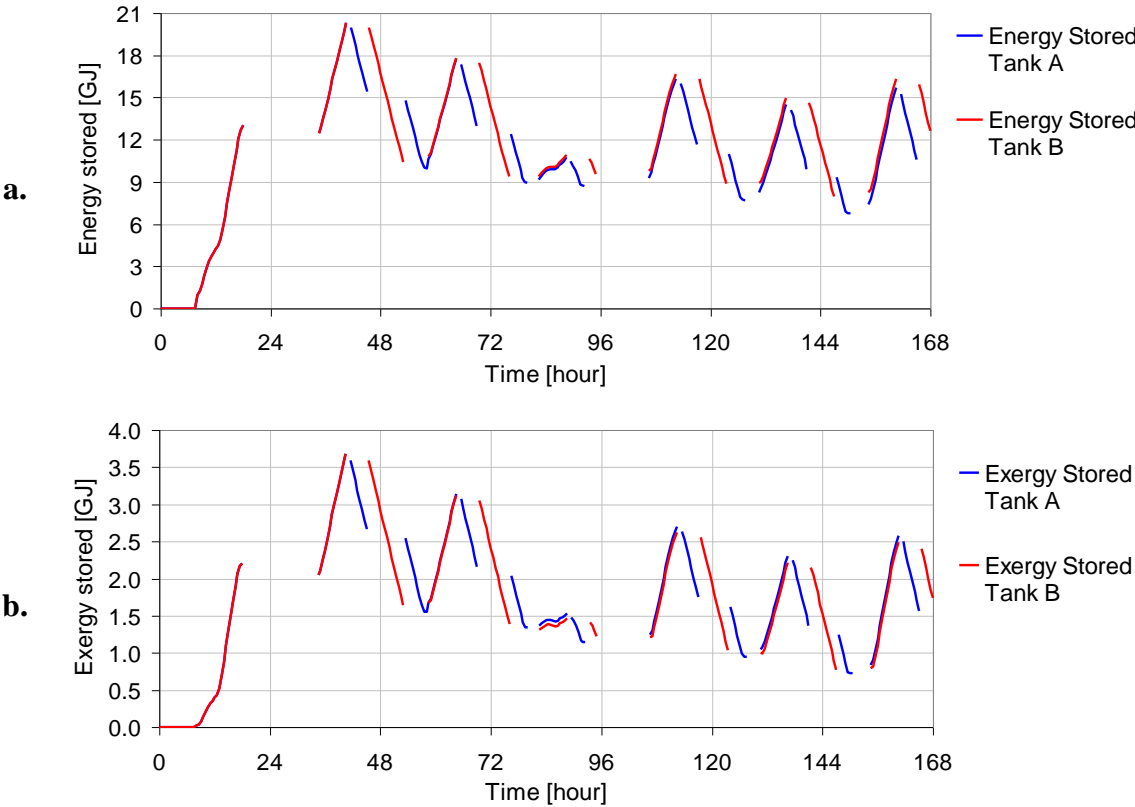
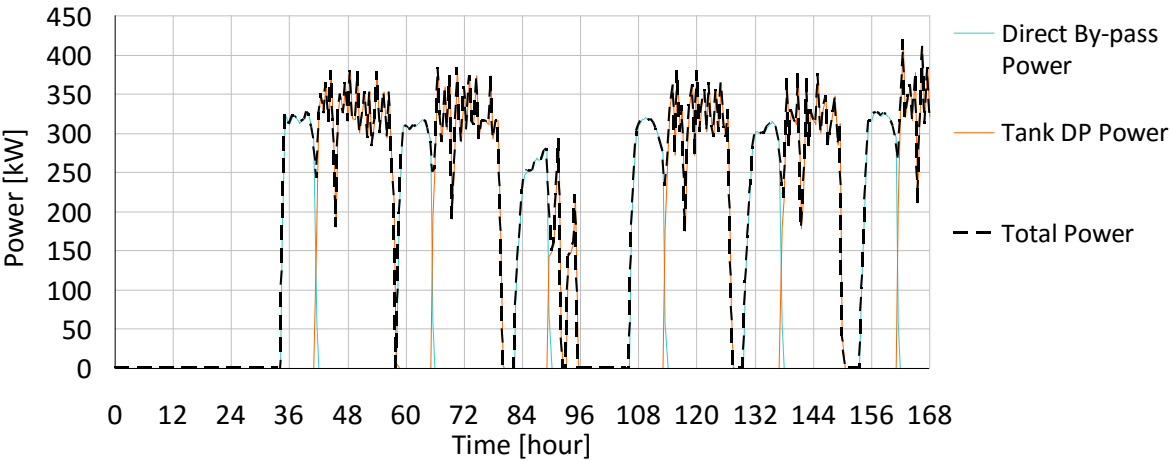


Figure 8



Tables:

Table 1 - Initial values and boundary conditions for the calculation.

	Charging $[x, \tau]$	Discharging $[x, \tau]$
PCM	$T_p[i, 0] = T_\infty$	$T_p[i, 0] = T_p[i, N_{t, \text{charg}}]$
	$\phi[i, 0] = 0$	$\phi[i, 0] = \phi[i, N_{t, \text{charg}}]$
HTF	$T_f[i, 0] = T_\infty$	$T_f[i, 0] = T_f[i, N_{t, \text{charg}}]$
	$T_f[0, j] = T_{\text{inlet}}$	$T_f[0, j] = T_{\text{inlet, discharg}}$
ST	$T_{st}[i, 0] = T_\infty$	$T_{st}[i, 0] = T_{st}[i, N_{t, \text{charg}}]$
Others	$E_{\text{stored}}[\tau = 0] = 0$	$E_{\text{stored}}[\tau = 0] = E_{\text{stored, charg}}$
	$\Xi_{\text{stored}}[\tau = 0] = 0$	$\Xi_{\text{stored}}[\tau = 0] = \Xi_{\text{stored, charg}}$

Table 2 – Data for LHS model validation

Parameters	Units	Value
PCM	-	Paraffin
Latent heat of fusion of PCM	J/kg	213000
Density of solid PCM	kg/m ³	861
Density of liquid PCM	kg/m ³	778
Specific heat of solid PCM	J/kgK	1850
Specific heat of liquid PCM	J/kgK	2384
Spheres diameter	m	0.055
HTF	-	Water
HTF Inlet Temperature	K	343
HTF flow rate	kg/s	0.033
Storage Tank Material	-	AISI316
Storage tank internal diameter	m	0.36
Storage tank length	m	0.46

Table 3 – Properties of the system components

Parameters	Units	Value
Solar collector total Aperture area (140 collectors)	m ²	2583
PCM Spheres diameter	m	0.04
PCM Melting Temperature	K	390
PCM latent heat	J/kg	3.3x10 ⁵
Density of liquid PCM	kg/m ³	1300
Density of solid PCM	kg/m ³	1480
Specific heat of solid PCM	J/kg-K	1383
Specific heat of liquid PCM	J/kg-K	2765
Storage Tank Material	-	AISI316
Storage tank internal diameter	m	2.5
Storage tank length	m	10

Table 4 – System operation phases referred to plant point indexes defined in Figure 4.

Hours of the day	Modules working	Notes
10 am - 5 pm	<ul style="list-style-type: none"> Tank A charging (V4 open) Tank B charging (V3 open) ORC constantly fed with by-pass flow rate (V2 open) 	<ul style="list-style-type: none"> Flow rate to ORC evaporator, $\dot{m}_{BP-ORC}=3\text{kg/s}$
5 pm -5.30 pm	<ul style="list-style-type: none"> ORC constantly fed with by-pass flow rate (only V2 open) 	<ul style="list-style-type: none"> Flow rate to ORC evaporator, $\dot{m}_{BP-ORC}=3\text{kg/s}$
5.30 pm - 9 pm	<ul style="list-style-type: none"> Only Tank A is discharged (V5 open – V6 closed) 	<ul style="list-style-type: none"> Discharge flow rate is constant, $\dot{m}_{DP}=4\text{kg/s}$ Tank inlet temperature during DP, $T_{DP}=370\text{K}$
9 pm - B/D/stop	<ul style="list-style-type: none"> Only Tank B is discharged (V6 open – V5 closed) 	<ul style="list-style-type: none"> Discharge flow rate is constant, $\dot{m}_{DP}=4\text{kg/s}$ Tank inlet temperature during DP, $T_{A-in}=370\text{K}$ Tank B discharge stops when $T_{B-out} < T_{melt,PCM}$
B/D/stop - 10 am	<ul style="list-style-type: none"> Only Tank A is discharged (V5 open – V6 closed) 	<ul style="list-style-type: none"> Discharge flow rate is constant, $\dot{m}_{DP}=4\text{kg/s}$ Tank inlet temperature during DP, $T_{A-in}=370\text{K}$ Tank A is discharged until $T_{A-out} > 370\text{K}$

Table 5 – Weekly averaged PCM Energy and Exergy Efficiencies for CP and DP

	Charging Phase		Discharging Phase	
	Tank A	Tank B	Tank A	Tank B
Average Energy Efficiency	83.4%	82.5%	92.6%	93.4%
Average Exergy Efficiency	69.1%	68.2%	66.7%	68.8%